

Demonstration of Damage-Free Mask Repair Using Electron Beam-induced Processes

Ted Liang, Alan Stivers, Michael Penn, Dan Bald and Chetan Sethi

Email: ted.liang@intel.com

Intel Corporation, 2200 Mission College Blvd., Santa Clara, CA 95054

Volker Boegli, Michael Budach, Klaus Edinger and Petra Spies

NaWoTec GmbH, 64380 Rossdorf, Germany

ABSTRACT

In this paper, we present the test results obtained from the first commercial electron beam mask repair tool. Repaired defect sites on chrome-on-glass masks are characterized with 193nm AIMS™ to quantify the edge placement precision as well as optical transmission loss. The electron beam mask repair tool is essentially based on a scanning electron microscope (SEM), therefore, it can be used for *in-situ* CD and defect metrology. E-beam for EUV mask defect repair is also discussed. These early results are very encouraging and demonstrate the basic advantages of electron beam mask repair as well as highlight the key challenge of charge control.

Key words: mask repair, electron beam induced etch and deposition, electron beam mask repair

INTRODUCTION

Due to the increased complexity of the mask features and the limited tool capability, mask repair of critical defects has become a delicate art in yielding useful masks. How well the mask shop performs the art depends on the capability of a suitable tool and the careful process that removes the defect with sufficient placement precision while at the same time preserves the optical properties of the repair site. There are four main figures of merit for characterizing a repair technology: 1) the versatility of being able to repair clear, opaque and phase defects; 2) the ability to control the repair as measured by placement precision; 3) spatial resolution measuring the ability to repair defects in tight spaces and on narrow lines on the mask per lithography design needs; 4) no damage to the mask in the repair process, including defect search, imaging and post repair measurements.

Three types of repair tools are currently employed for production in the mask shop and they are respectively based on laser removal, FIB (focused ion beam) deposition and etch, and AFM-based mechanical cut. Each of them has unique advantages and significant limitations and, obviously, no one has all the traits described above. FIB tools are commonly used for both etch and deposition applications of mask defect repair. However, substrate damage from Ga ion implantation is a fundamental problem for FIB. It becomes increasingly difficult to control optical transmission loss due to ion implantation, particularly for phase shifting masks and high MEEF features on binary masks.

One way to avoid substrate damage is to replace Ga ions with electrons. Electron beams have the additional advantage of excellent spatial resolution. We have demonstrated the feasibility of electron beam induced chemical reactions for both deposition and etching that can be used for repairing mask defects [1, 2]. We also reported that electron exposure in repair conditions indeed causes no damage to mask substrates [3]. We believe and will further demonstrate in this paper that e-beam mask repair technology attains all four merits and will be the technology of choice for mask repair in meeting the challenging requirements for future generation nodes.

The damage-sensitive Mo-Si multilayers on the mask blanks for extreme ultra-violet (EUV) lithography make the true damage-free nature of the electron beam essential for EUV mask repair. For EUV mask, the inspectability and repairability of pattern defects are two main factors in determining the types of materials that can be employed for absorber layer. For pattern defect inspection, absorber materials and surface treatment can be used to ensure high image

contrast for optical inspection and our DUV inspection results of programmed defect masks showed that EUV masks are as inspectable as conventional binary Cr masks [4, 5]. For defect repair, we reported excellent e-beam etch rate and selectivity of TaN versus buffer layer SiO₂ [1] and capping layer Ru (this paper). E-beam mask repair technology not only provides damage-free defect repair, more importantly, it also makes possible a new EUV mask architecture in which a buffer layer is no longer needed. This enables new EUV mask architectures such as those where the buffer layer is replaced with a Ru capping layer [6]. This could not be possible if FIB repair were used since the ions would be implanted into the ML through a 2-4nm Ru layer.

A few years ago [7], we advocated the use of electrons for mask repair based on the facts described above that e-beam can induce deposition and etch. The key advantage of e-beam mask repair is the damage-free nature of the electrons. One can image the mask with any number of scans without worrying about damaging the mask. The high resolution, the ease of adjusting the magnification and searching for defects make the e-beam tool far easier to use as compared with an AFM-based tool. Another damage-free aspect of e-beam repair is the pure chemical nature of the e-beam induced etching process (versus FIB where sputtering can be a main removal mechanism). With proper selection of gases one can develop etching processes of high selectivity that only remove the defect material without adverse effect. We believe that the combination of dual capabilities with damage-free processes provide the industry a promising technology of unmatched potential as compared with laser, ion or mechanical tip based platforms. To demonstrate the feasibility we have successfully deposited nano-features on the mask for clear defect repair and etched different materials for opaque and phase defect repair.

To transition from a feasibility study to the development of a repair technology that can be implemented in manufacturing we have installed the industry's first commercial e-beam mask repair tool that meets SEMI S2/S8 standards and manufacturing clean room requirements.

In addition to its repair capabilities, the e-beam tool is also a fully functional SEM that can be used for any metrology applications of a standard CD-SEM – one tool can serve the purpose of repair and CD metrology. Unlike FIB where one has to be very careful in limiting the number of scans during imaging as not to cause unacceptable transmission loss from Ga staining, e-beam system offers this unparalleled metrological benefit for imaging mask features as well as for characterizing defects.

In this paper, we describe the e-beam mask repair system and highlight the tool's main functionalities, including the electron column, a MultiJet gas delivery system, the laser interferometer-controlled precision stage, and a GUI-controlled beam scan software. We then present the repair data as characterized by AFM, SEM, and 193nm AIMS™.

SYSTEM DESCRIPTION

The mask repair system is based on a leading edge SEM, with the addition of a planar 6-inch laser interferometer stage and a five channel gas injection system [2]. With its combined electrostatic and electromagnetic lens the GEMINI column is optimized for high spatial resolution at the low electron energies that are important for mask repair. To reduce sample charging by dynamically balance the charge, the landing energy of primary electrons should be around the E2 energy at which total electron yield from the surface is 1, i.e., the number of backscattered and secondary electrons roughly equals to the number of incident primary electrons. For quartz surfaces, the range of E2 is about 0.8keV to 1keV. For photolithography masks, the system is mostly operated at around 1keV. However, the electron energies can be continuously varied in 10eV steps from 200eV to 30keV. The column is also differentially pumped to allow the introduction of low pressure gases into the specimen chamber. With this added capability the system can be operate at low variable pressure up to 100Pa in the chamber.

The microscope is equipped with a gas supply system able to deliver up to five process gases in any combination desired for electron beam induced reactions. It can handle solid and liquid precursors as well as gases in pressurized cylinders. The gases are installed in a gas cabinet near the tool. The gas cabinet design allows the flexibility of installing different gases for testing various etching and deposition processes. The uniform delivery of process gases to the repair site on the mask is turned on and off by software controlled fast-reacting mini-valves inside the vacuum chamber. This allows relatively low gas retention time as well as fast switching of gases. The gas flow at the sample is either controlled by mass flow controller or temperature regulators depending on the types of gases.

The system is operated by an integrated mask repair software with a work flow oriented GUI. All sub-systems including beam scanning and gas delivery are fully software controlled. Secondary electron signal can be used for endpoint detection, and has been shown to be quite effective for some materials. For improved edge placement precision an image processing based drift correction system can be employed. The system is installed in the clean room in a typical bay-chase configuration as shown in Figure 1.

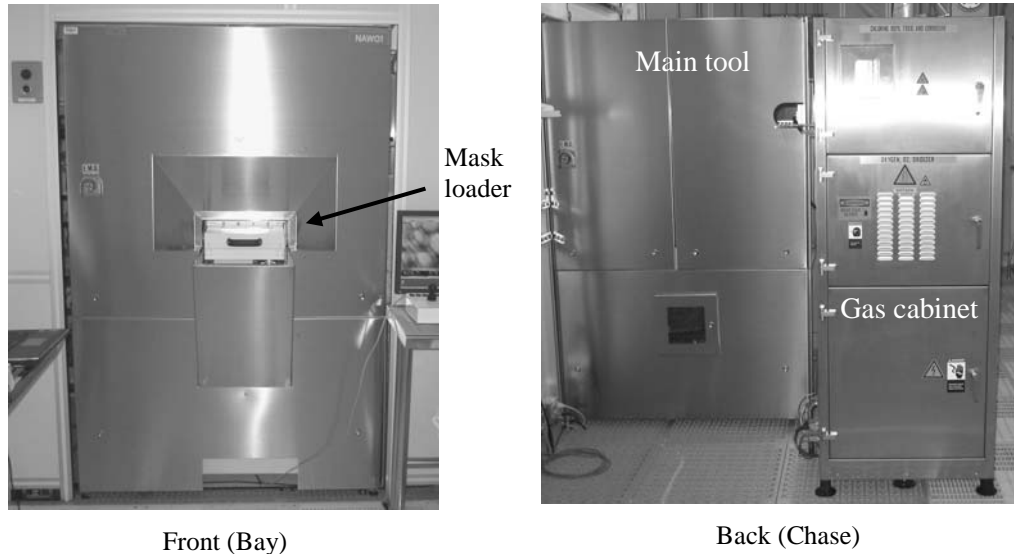


Figure 1: The e-beam repair tool is bulk-head mounted in the clean room (left). A gas cabinet (right) is used for storing the materials that are delivered to the vacuum chamber via gas channels through the MultiJet.

CLEAR DEFECT REPAIR

Deposition is used for clear defect repair where carbon or metallic compounds are formed when the site is illuminated with electrons in the presence of a precursor gas. In our case, platinum (Pt) organometallic precursor (methylcyclopentadienyl platinum – $(CH_3C_5H_4)Pt(CH_3)_3$, a commonly used precursor [8]) is used for depositing Pt in the form of Pt and carbon mixture (simply referred as Pt/C in this paper). The actual composition of the deposited film on the surface depends on the type of precursors, e-beam parameters and gas conditions used. For some applications it is desirable to deposit metallic films. However, for binary mask repair the composition of deposited materials is less important as long as it provide chemical and optical reliability since practically most depositions produce optically opaque materials.

The deposition rate is quite good, and appears to be linear as a function of electron dose with a short initial delay as shown in Figure 2, which plots the height of a $1\mu m \times 1\mu m$ area measured by AFM as a function of e-beam scan time. The observation of a delay time probably depends on the surface conditions. The deposition rate calculated from these measurements is $0.014\mu m^3/nC$. It is generally reported that the yield of e-beam induced deposition is lower than that of ion beam for large area depositions where the flux of precursor gas is not limiting the process. This is not a concern for mask repair because of the fact that much higher e-beam current than ion current can be used for the same beam size and actual deposition time is usually not a main contributor for repair throughput time.

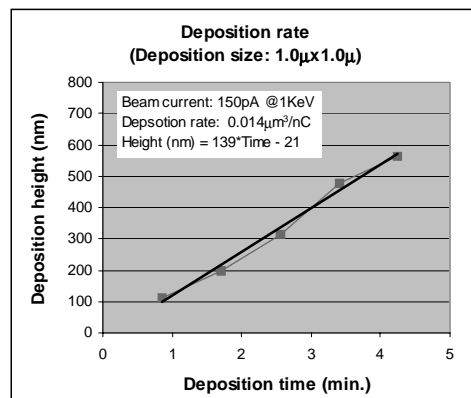


Figure 2: Deposition heights of $1\mu m \times 1\mu m$ feature vs. e-beam exposure time. The deposition rate calculated from these measurements is $0.014\mu m^3/nC$.

Clear defect repair by deposition is characterized with SEM and 193nm AIMS™ to determine edge placement precision and repair offset. As an example, Figure 3 shows a programmed clear defect before and after repair for a binary Cr-on-glass (COG) mask. The Cr line width is 620nm. The repair box was drawn larger than the defect. We targeted to make a deposition to fill up the clear defect to about the same height as the Cr line, i.e., about 100nm thick of Pt/C. Figure 3d) displays the AFM-measured heights at two different points marked as (A) and (B) and they are 113.5nm and 13nm, respectively. The deposition height of 113.5nm is essentially the same as our target.

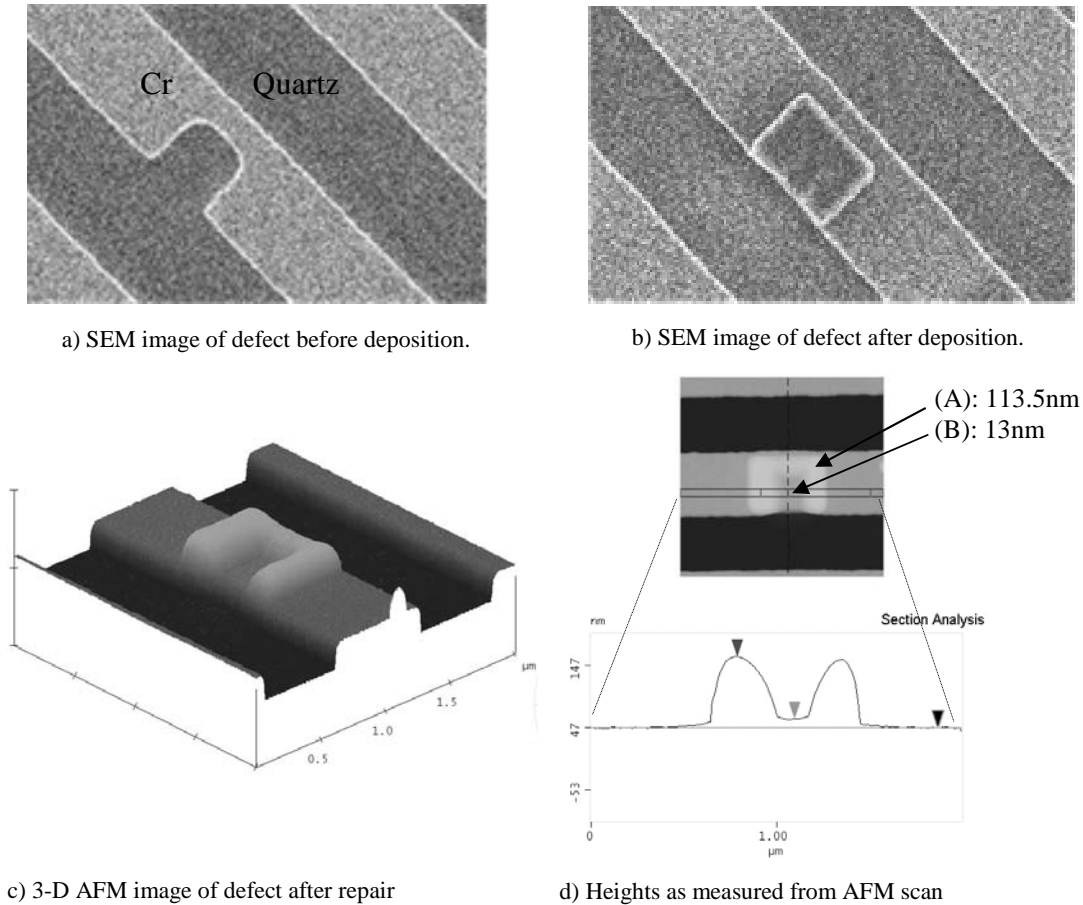
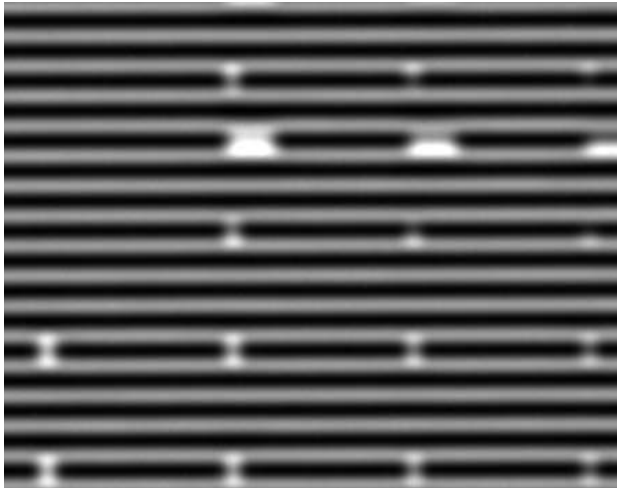


Figure 3: SEM and AFM micrographs showing defect site before and after repair. The width of the equal lines and spaces is 620nm (4X). The AFM-measured deposition height is 113.5nm.

EDGE PLACEMENT PRECISION

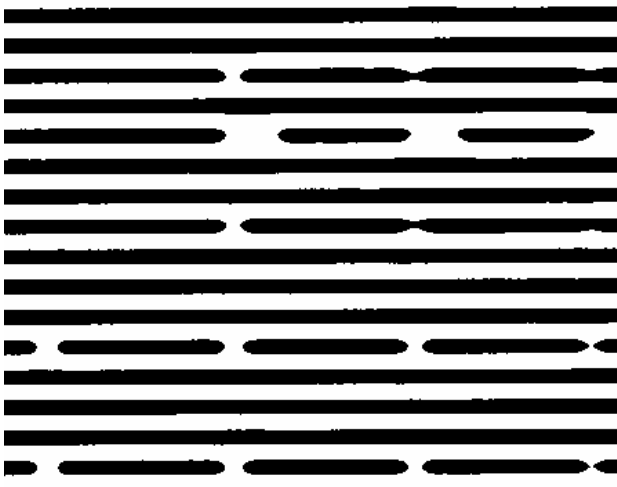
One of the critical repair qualities is edge placement deviation (EPD). The best measure for EPD is the placement precision determined from the CD variations at the repair site as compared to the defect-free reference CD. In our case, we measure CDs from the mask aerial images taken with 193nm AIMS™. Figure 4 shows the aerial image of a portion of the programmed defect mask with some defects before and after repair. A stepper-equivalent numerical aperture (N.A) of 0.75 is used for taking these images. An intensity threshold value of 0.33 is used for CD measurements. This threshold value is calibrated to produce equal lines and spaces of targeted CDs on the resist wafer.



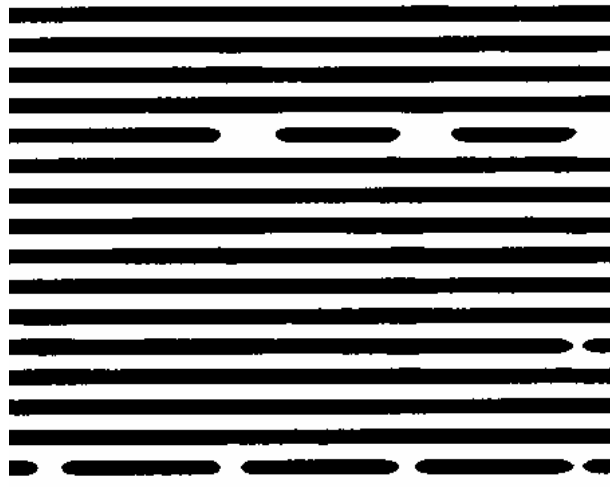
a) Aerial image before repair



b) Aerial image after the repair of nine defects



c) Intensity threshold image before repair



d) Intensity threshold image after repair.

Figure 4: 193nm AIMSTM images take before and after repair for some defects. 0.75NA is used. A threshold value of 0.33 is used for displaying the images in c) and d).

To determine a repair EPD by analyzing the threshold aerial images, we overlay and align the two images, one taken at the reference site and one taken at the defect site. The reference site has the same features as the defect site just without the defects. Then we subtract the reference image from the defect image. The resulting difference image, shown in Figure 5 as an example, displays all the information needed for the analysis. Since the Cr lines and spaces are represented as dark and white pixels, respectively, in the threshold images (see Figure 4), the gray regions in the reference image in Figure 5 represent a perfect match of lines (dark gray) and spaces (lighter gray), and the dark regions indicate that the defect image has extra dark pixels – extra Cr or extra deposition in the case of clear defect repair. Obviously, the white regions in the differential image indicate that missing Cr or more deposition is needed for a perfect clear defect repair. Thereby, width of the white or dark regions on the differential image directly measures the EPD.

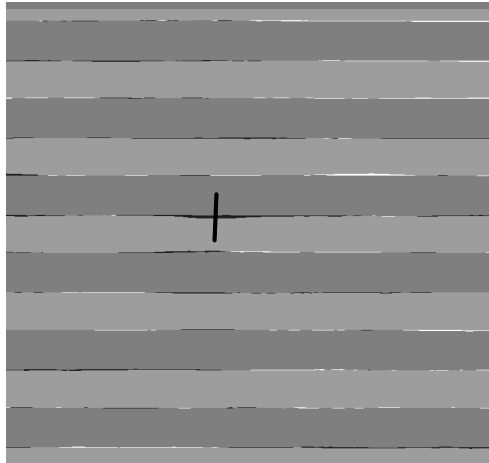


Figure 5: Differential AIM image used for measuring the edge placement errors. The dark and white regions indicate extra and missing Cr, respectively. See text for details.

The extracted EPDs from the analysis of 14 defect repairs are plotted in Figure 6a). The average EPD is 38nm and the placement precision is 33nm (3σ). While the EPD can be corrected by biasing the repair setup, the control of precision is affected by many factors, and among others, such as system drift and manual or automatic repair box placement, the biggest one is e-beam drift caused by surface charging, which is also the foremost problem for the measurement precision in a CD-SEM. Surface charging is a major cause of placement errors and the effect can be clearly demonstrated by comparing Figures 6a) with 6b). Figure 6b) is a plot of EPDs of 14 repairs on a programmed EUV defect mask, which has much less charging than the COG mask. The placement precision calculated from SEM measured EPDs is 8.9nm (3σ).

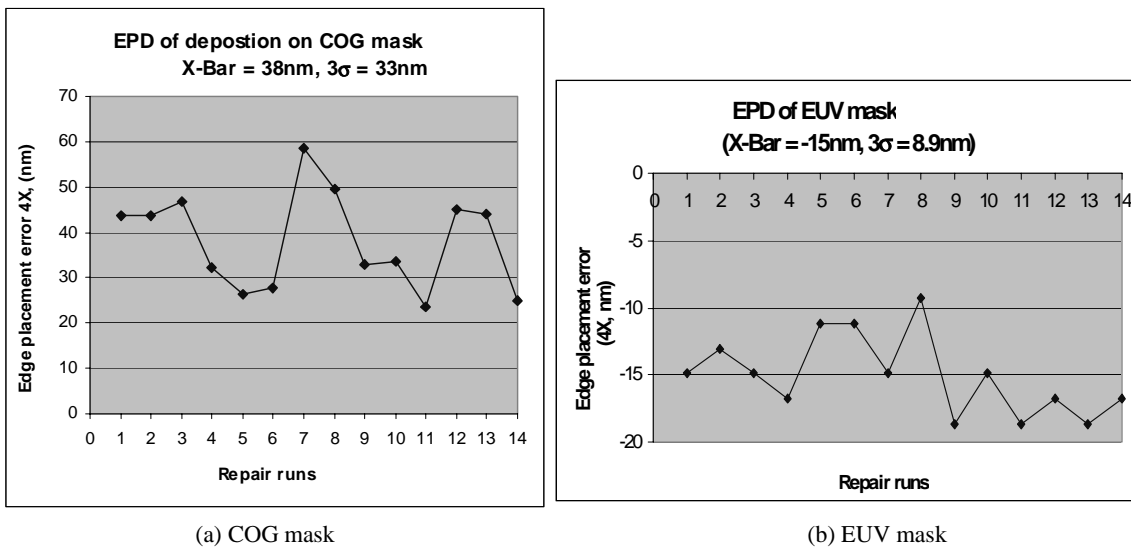


Figure 6: Plots of EPDs measured from repairing 14 programmed clear defects. All the values are 4X numbers. The average EPDs for COG and EUV masks are 38nm and -15nm, respectively, and they can be corrected by placement bias.

CHARGE COMPENSATION TO IMPROVE PLACEMENT PRECISION

When charges build up at the mask surface, the surface potential affects the landing voltage of the primary electron beam and causes the beam focus and magnification to vary. The surface of quartz based masks (binary COG or PSMs) can be either charged positively or negatively, depending on the primary electron energies used relative to E2. Charging problem is worse for repair than for imaging in CD-SEM operations since in repair the beam scans in a very small area, thus dumping a lot of charge within a tiny area. A feedback loop of drift correction alone is not sufficient to solve the problem and sometimes it is not possible to make drift correction because charging (or discharging) is not a predictable process.

Charge control or compensation presents the most critical challenge in enabling e-beam to meet the repair placement requirements. We are evaluating different ways of charge mitigations and preliminary results are encouraging [9]. Figure 7 is a plot of the distance (represented in x and y coordinates) of the electron beam drifted during deposition intervals. The interval is about 3 seconds. Surface charging causes the beam to drift randomly in a large range from 50nm up to more than 200nm (represented by the square data points) without charge compensation mechanism. With charge compensation, the beam is stable to within about 3-5nm as shown by the solid circular data points. With this capability, the precision of repair edge placement is expected to be about 5nm (3σ).

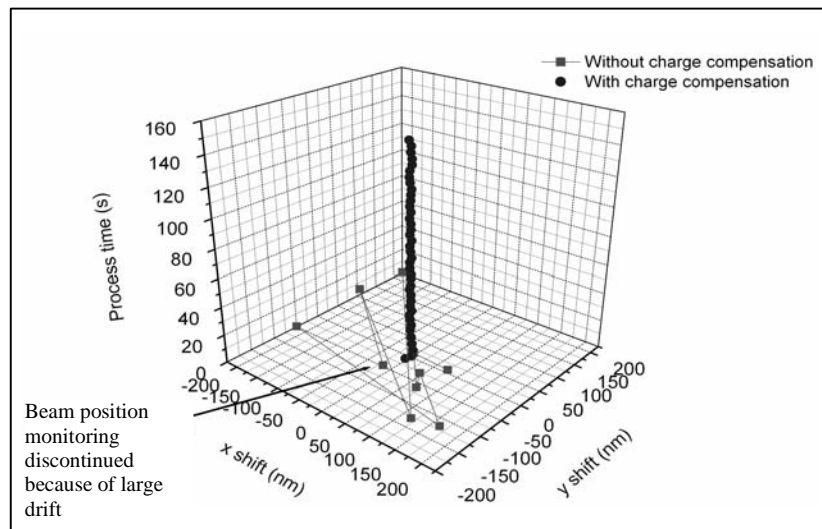


Figure 7: Comparison of electron beam drifts as measured by the image position (x, y coordinates) change on the mask surface with (solid circle data points) and without (solid square data points) charge compensation. Only few points were recorded without charge compensation due to large drift as noted in the plot. With charge compensation, the beam is very stable, the drift is less than 5nm between monitoring intervals of about 3 seconds.

CLEANING COMPATIBILITY OF DEPOSITION

A great variety of materials can be deposited with e-beam and almost every material has enough optical density to be used for clear defect repair. However, material durability in mask cleaning determines which material is good. We have started testing of Pt/C for chemical durability in standard acid cleaning process. After one cycle of cleaning, a 2nm Pt/C is lost determined by comparing the AFM heights of the same deposition before (Figure 3) and after cleaning as shown in Figure 8. Assuming a constant rate of material loss per clean cycle, Pt/C deposition is expected to be compatible with mask clean chemistries. More cleaning tests are in progress

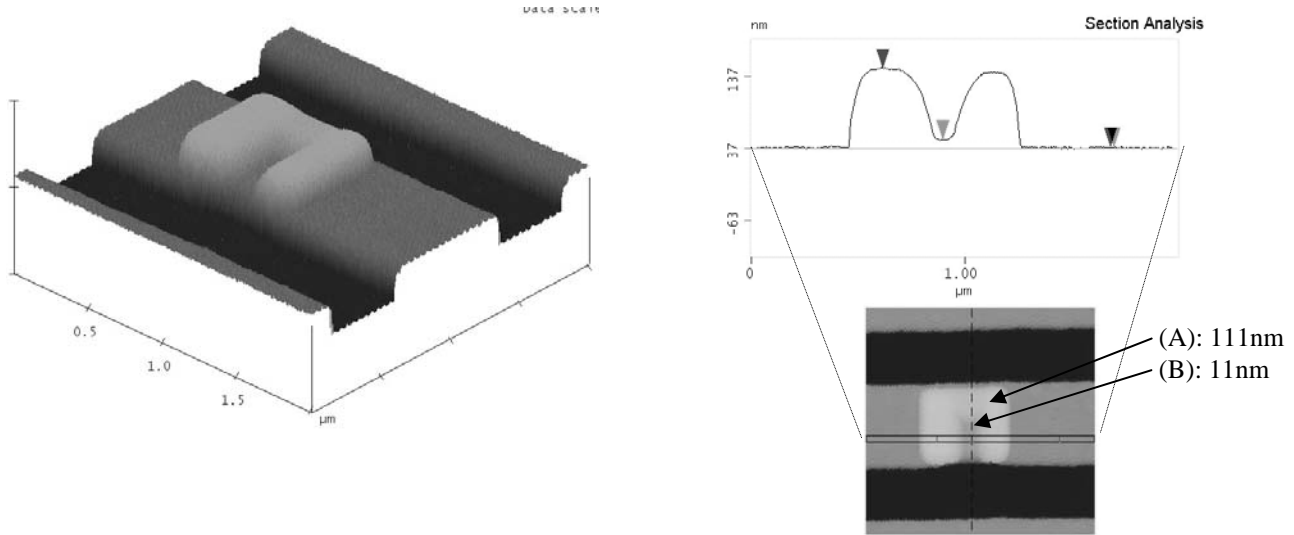


Figure 8: AFM image of repair site after a standard acid clean cycle. Only 2nm Pt/C was eroded, indicating that the deposition is durable enough to be used for clear defect repair.

HIGH SPATIAL RESOLUTION OF E-BEAM REPAIR

Another important figure of merit for a good repair technology is its spatial resolution – the capability of repairing defects in tight spaces, both lateral and vertical. Among all energized particles of photons, ions and electrons used for fabrication of nano-structures, focused electron beam produces the smallest features by deposition or etching. We as well as others [10] have reported that dot and line features as small as 15nm in lateral dimensions could be deposited. For example, Figure 10a) is an SEM micrograph showing two lines formed from Pt/C deposition of widths of about 27nm and 230nm, respectively. Note that the finely defined edges of the depositions will enable very accurate pattern generations for mask repair.

Similar to deposition, equally small features have also been etched. A 30nm wide line was etched into 75nm thick TaN film as displayed by the SEM and AFM images in Figure 9b). Due to its tip size, AFM can not reach the bottom of the etched line as shown by the 3-D AFM image in Figure 9b).

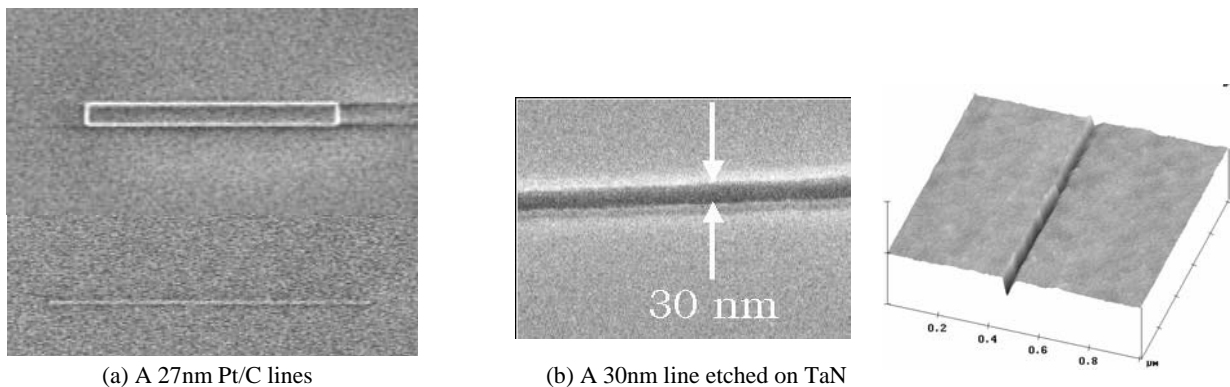


Figure 9: Examples of e-beam deposited and etched fine lines around 30nm, indicating e-beam provides high spatial resolution for mask repair.

With such high special resolution for both deposition and etching, we expect that e-beam mask repair technology will meet the requirements for several generations of lithography nodes in the future.

HIGH ETCH SELECTIVITY FOR EUV ABSORBER REPAIR

TaN-based materials have been accepted as the materials of choice for EUV absorber. E-beam provides excellent selectivity for etching TaN absorber patterned on either SiO₂ buffer layer or Ru capping layer. We reported [1] about 20:1 etch selectivity of TaN vs. SiO₂. Here we report even better selectivity of TaN vs. Ru. Figure 10 is an AFM 3-D image of an etched TaN line on Ru, where a rectangular area (the dotted box in Figure 10) covering both the Ru and TaN layers was etched until the 75nm thick TaN was completely etched away. The AFM measured depth of etched Ru is about 1nm, showing about 75:1 etch selectivity.

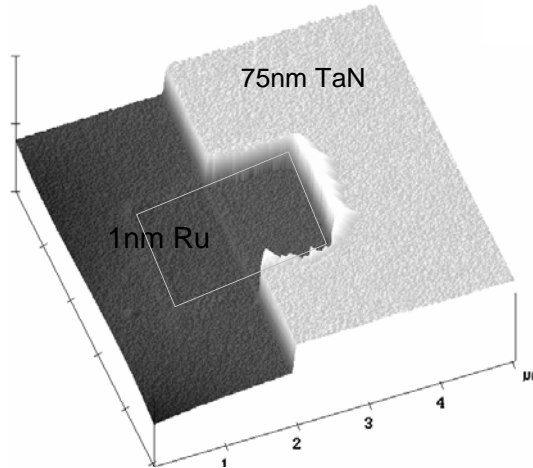


Figure 10: 3-D AFM image showing e-beam etching of TaN on Ru with excellent etch selectivity of TaN against Ru. The dotted rectangular box outlines the etched area covering both TaN and Ru for easy measurements of etch selectivity.

SUMMARY

In this paper, we have reported repair data using e-beam induced deposition and etching for both COG and EUV masks. The results demonstrated that e-beam based deposition and etching is a viable technology that offers an exciting solution for mask repair with all four important characteristics of an ideal repair technology: 1) versatility that works for clear, opaque and phase defects, 2) good edge placement control, 3) high spatial resolution, and 4) damage-free repair. We have achieved edge placement precision (3σ) of 33nm and 10nm for COG and EUV masks, respectively. Lines narrower than 30nm can be readily deposited and etched.

Mask charging remains a key challenge for employing the fullest potential of e-beam mask repair technology. We are working on solutions for charge compensation to mitigate the charging effects on beam drift and preliminary results are encouraging. Once the charging issue is resolved, we believe that e-beam induced processes will provide us with an innovative and robust technology for meeting the mask requirements for the next several generation nodes.

ACKNOWLEDGEMENTS

We would like to express our thanks to Saghir Munir, Vikram Tolani, Edgar Buenconsejo and Chanh Ly for their support on AIMSTM and AFM data collection and analysis.

REFERENCES

1. Ted Liang and Alan Stivers, "Damage-free Mask Repair Using Electron Beam Induced Chemical Reactions", SPIE Proc., Vol. 4688, p. 375-384 (2002).

2. Klaus Edinger, Hans Becht, Rainer Becker, Volker Bert, Volker Boegli, Michael Budach, Susanne Göhde, Jochen Guyot, Thorsten Hofmann, Ottmar Hoinkis, Alexander Kaya, Hans W.P. Koops, Petra Spies, Bernd Weyrauch, "A Novel Electron-beam-based Photomask Repair Tool", SPIE Proc., Vol. 5256, p.1222-1231 (2003).
3. Ted Liang, A. Stivers, G. Liu, G. Dao, V. Liberman, M. Rothschild, S.T. Palmacci and L. Scipioni, "Evaluation of 157nm substrate damage during repair", 2nd Int'l. Symp. on 157nm Lithography, Dana Point, CA (May 2001).
4. Ted Liang, Alan Stivers, Pei-Yang, Yan, Edita Tejnjl and Guojing Zhang, "Enhanced Optical Inspectability of Patterned EUVL Mask," SPIE Proc., Vol. 4562, 288 (2002).
5. Donald Pettibone, Andrei Veldman, Ted Liang, Alan R. Stivers, Pawitter Mangat, Bing Lu, Scott Hector, James Wasson, Kenneth Blaedel, Emily Fisch, and David M. Walker, "Inspection of EUV Reticles", SPIE Proc., Vol. 4688, 363 (2002).
6. Pei-Yang Yan, Guojing Zhang, Eberhard Spiller and Paul Mirkarimi, "Ru capped EUVL ML mask blank performance", in his proceedings.
7. Ted Liang, Alan Stivers, Rick Livengood, Pei-Yang Yan, Goujing Zhang and Fu-Chang Lo, "Progress in extreme ultraviolet mask repair using a focused ion beam", J. Vac. Sci. Technol., **B18**(6), 3214 (2000).
8. Hans Koops, Johannes Kretz, Michael Rudolph, Markus Weber, Gerold Dahm and Kam Lee, Jpn. J. Appl. Phys., "Characterization and Application of Materials Grown by Electron-Beam-Induced Deposition "Vol. 33, 7099 (1994).
9. Klaus Edinger, et al, "performance results from our novel electron beam based photomask repair tool" in this proceedings.
10. David Joy (Private communications).